

WEATHERGFM: LEARNING A WEATHER GENERALIST FOUNDATION MODEL VIA IN-CONTEXT LEARNING

Xiangyu Zhao^{1,2}, Zhiwang Zhou¹, Wenlong Zhang^{1,✉}, Yihao Liu¹, Xiangyu Chen¹,
 Junchao Gong^{1,3}, Hao Chen¹, Ben Fei¹, Shiqi Chen⁴, Wanli Ouyang¹,
 Xiao-Ming Wu^{2,✉}, Lei Bai¹

¹Shanghai AI Laboratory ²The Hong Kong Polytechnic University

³Shanghai Jiao Tong University ⁴Shanghai Meteorological Service

zhangwenlong@pjlab.org.cn, xiao-ming.wu@polyu.edu.hk

ABSTRACT

The Earth’s weather system encompasses intricate weather data modalities and diverse weather understanding tasks, which hold significant value to human life. Existing data-driven models focus on single weather understanding tasks (e.g., weather forecasting). Although these models have achieved promising results, they fail to tackle various complex tasks within a single and unified model. Moreover, the paradigm that relies on limited real observations for a single scenario hinders the model’s performance upper bound. In response to these limitations, we draw inspiration from the in-context learning paradigm employed in state-of-the-art visual foundation models and large language models. In this paper, we introduce the first generalist weather foundation model (WeatherGFM), designed to address a wide spectrum of weather understanding tasks in a unified manner. More specifically, we initially unify the representation and definition of the diverse weather understanding tasks. Subsequently, we devised weather prompt formats to manage different weather data modalities, namely single, multiple, and temporal modalities. Finally, we adopt a visual prompting question-answering paradigm for the training of unified weather understanding tasks. Extensive experiments indicate that our WeatherGFM can effectively handle up to ten weather understanding tasks, including weather forecasting, super-resolution, weather image translation, and post-processing. Our method also showcases generalization ability on unseen tasks.

1 INTRODUCTION

Modeling Earth weather systems involves a series of complex subprocesses that are intended to transform intricate Earth observation data into applications like weather forecasting (Chen et al., 2023a; Bi et al., 2023a), downscaling (Chen et al., 2022; Xu et al., 2024; Ling et al., 2024; Liu et al., 2024c), assimilation (Huang et al., 2024; Wang et al., 2024b), retrieval (Liu et al., 2011), and bias correction (Gong et al., 2024a;b). During the past decade, many data-driven methods have been investigated for various weather understanding tasks and delivering desirable performance on specific tasks. For example, recent studies using large-scale data (e.g., ERA5 reanalysis data (Hersbach et al., 2020)) have exceeded the accuracy of conventional numerical weather forecasts. However, current weather foundational models face challenges regarding generalizability and data scale limitations. On the one hand, the Earth observation system consists of a variety of observation devices, such as satellites, radar, and weather stations, which produce diverse modalities of data. Consequently, designing a specific model for a single-task scenario is highly complex, time-consuming, and labor-intensive. On the other hand, large-scale data in fields such as computer vision can be obtained at a low cost, whereas weather understanding tasks face an intrinsic bottleneck in data scale due to restrictions on individual scenes and single observation devices as shown in Table 1. For instance, local short-term precipitation forecasting models can only utilize a finite range of observational data.

A significant trend in AI research is the development of foundation models, shifting towards large-scale pre-training and in-context learning. This paradigm enables unified processing of a

✉ Corresponding author.

Table 1: Comparison of existing task-specific and general models across Earth science and computer vision fields. Our WeatherGFM demonstrates its ability to handle multi-tasks, multi-modal data, and general capabilities, showcasing its strength in acquiring hard-to-access weather data.

| Category | Method | Data Acquisition Difficulty | Supported Tasks | Multi-tasks support? | Multi-modal support? | Generalist support? |
|-----------------|-------------------------------|-----------------------------|---|----------------------|----------------------|----------------------|
| Computer Vision | HAT (Chen et al., 2023d) | Low-cost | Image super-resolution (SR) | ✗ | ✗ | ✗ |
| | IPT (Chen et al., 2021) | Low-cost | Image restoration, Derain, Dehaze | ✓ | ✗ | Requires fine-tuning |
| | Painter (Wang et al., 2023a) | Low-cost | Image restoration Segmentation, Keypoint detection | ✓ | ✗ | ✓ |
| | PromptGIP (Liu et al., 2023a) | Low-cost | Image restoration, Derain, Dehaze | ✓ | ✗ | ✓ |
| | GenLV (Chen et al., 2024a) | Low-cost | Image restoration, enhancement, translation | ✓ | ✗ | ✓ |
| Earth Science | Prediff (Gao et al., 2024) | High-cost | Weather forecasting | ✗ | ✗ | ✗ |
| | Cascast (Gong et al., 2024a) | High-cost | Post-processing | ✗ | ✗ | ✗ |
| | Climax (Nguyen et al., 2023) | High-cost | Weather forecasting, Weather image SR | ✓ | ✗ | Requires fine-tuning |
| | Aurora (Bodnar et al., 2024) | High-cost | Weather forecasting Atmospheric chemistry prediction | ✗ | ✓ | Requires fine-tuning |
| | WeatherGFM (ours) | High-cost | Weather forecasting, Weather image SR Weather image translation, Post-processing | ✓ | ✓ | ✓ |

multitude of complex tasks and generalization to unseen tasks. For example, large language models (LLMs) can perform a variety of language-centric tasks (e.g., question answering, machine translation and dialogue state tracking (Feng et al., 2023)) by combining language input-output examples with new query inputs (prompts) without optimizing model parameters (Brown, 2020). Similarly, vision foundation models (Wang et al., 2023b; Chen et al., 2024b) employ visual prompts with query inputs to carry out diverse image-centric tasks, such as semantic segmentation, depth estimation, and image restoration. These studies highlight the significant potential of generalist foundational models.

The study of foundation models remains largely limited in weather understanding, with the majority focused on Computer Vision and Natural Language Processing. While there has been some progress with large foundation models in weather and climate, the focus is mainly on weather forecasting and downscaling tasks. For example, Climax (Nguyen et al., 2023) uses a pre-training-finetuning paradigm for weather forecasting and downscaling. Aurora (Bodnar et al., 2024) employs LoRA to unify weather forecasting and quick prediction of atmospheric chemistry. However, as shown in Table 1, these studies do not take into account the modeling of multi-modalities and multi-tasks. This poses a challenge: *Is it possible to design a universal foundation model capable of handling the variety of complex weather understanding tasks and data modalities?*

In this paper, we first propose a weather generalist foundation model, WeatherGFM, to uniformly address a variety of complex weather understanding tasks and data modalities. Unlike prior studies that focused on weather forecasting, our proposed method can expand the task scope to weather forecasting, weather super-resolution (i.e., weather downscaling), weather image translation (i.e., synthetic weather radar) (Veillette et al., 2020), and post-processing (Gong et al., 2024a). These tasks all belong to the domain of weather understanding, but their modalities are distinct. Specifically, Sequence modal data can be utilized for weather forecasting, such as short-term predictions based on radar data. Multi-modal data can be employed for weather image translation, such as converting multi-modal satellite data to generate radar data. Single-modal data can be applied to various common scenarios, such as radar image super-resolution and post-processing. To unify the diverse weather data modalities into a general representation, we introduce a weather prompt format that assigns different prompt phrases to various modalities. By leveraging in-context learning, our WeatherGFM achieves a promising in-context ability on both various seen tasks and unseen tasks. The significance of our work can be summarized as:

- We propose the first weather generalist foundation model (i.e., WeatherGFM), which can handle more than ten weather understanding tasks.
- Our weather prompt design supports a diversity of weather data modalities, including time-series, multi-modal, and single-modal data.
- Our WeatherGFM with in-context learning first demonstrates the generalization ability to unseen weather understanding tasks.

2 RELATED WORK

Weather understanding and beyond. Over the past decade, machine learning techniques (Zhang et al., 2022; 2023; 2024; Wang et al., 2024a) applied in vision tasks have continuously drawn attention within the field of weather and climate. Numerous data-driven machine learning models have been proposed to address classical tasks in weather understanding (Veillette et al., 2020), such as forecasting, super-resolution, image translation, and post-processing. Weather forecasting (Bi et al., 2023a) aims to predict future observations from past data. Weather super-resolution tasks, i.e., weather downscaling, Chen et al. (2022) focus on recovering high-resolution data from low-resolution observations. Weather image translation tasks (Stock et al., 2024) involves converting existing observational data into desired target modalities, such as transforming satellite observations into ground-based weather radar data. Post-processing tasks seek to enhance existing model results, such as bias correction and deblurring (Gong et al., 2024a;b).

Despite significant advancements, current methods often rely on specialized datasets and customized single-task models for certain scenarios. Consequently, single-task models struggle to exhibit strong generalization abilities and fail to capture the interconnections between diverse tasks, which hinders the establishment of simulations for the Earth system.

Weather foundation model. The rise of foundation models in Natural Language Processing and computer vision has sparked interest in their application for weather and climate. Large foundation models, enhanced through pre-training, improve the generalization of AI climate models and can be fine-tuned for specific tasks. Pathak et al. (2022) proposed FourCastNet, a climate pre-trained model using Vision Transformer for high-resolution predictions and rapid inference through self-supervised pre-training and autoregressive fine-tuning. Pangu-Weather (Bi et al., 2023a) utilizes a 3D Earth-specific Transformer for accurate global predictions. FengWu series (Chen et al., 2023a; Han et al., 2024) solve the forecast problem from a multi-modal and multi-task perspective. ClimaX (Nguyen et al., 2023) introduces supervised pre-training to weather prediction, offering flexibility for diverse forecasting tasks. W-MAE (Man et al., 2023) employs unsupervised training via a Masked Auto-Encoder, while MetepFL (Chen et al., 2023b) and FedWing (Chen et al., 2023c) advocate for prompt-based federated learning to enhance collaborative training while protecting privacy. Recent advancements, such as OceanGPT (Bi et al., 2023b), extend LLM capabilities to ocean-related tasks, and ClimateBERT (Webersinke et al., 2021) focuses on processing climate-related texts from extensive sources.

Visual in-context learning. In recent advancements, visual in-context learning has emerged as a promising research area, inspired by the success of language models like GPT-3 (Brown, 2020). These models adapt to various NLP tasks using prompts or in-context examples without extensive retraining. Similarly, in the vision domain, models such as MAE-VQGAN (Hojel et al., 2024) and Painter (Wang et al., 2023b) have begun exploring in-context learning. However, challenges persist, especially in low-level tasks requiring detailed pixel manipulation. To address this, PromptGIP (Liu et al., 2023b) and GenLV have incorporated in-context learning concepts into their designs to unify low-level vision tasks with diverse input and output modalities, aiming to develop generalist models. Vision-language models (Liu et al., 2024a;b; Zhao et al., 2024a;b) like Unified-IO (Lu et al., 2022) and Unified-IO 2 (Lu et al., 2024) have made significant progress in integrating multiple tasks, highlighting the potential for unified approaches across modalities. Additionally, compositional visual reasoning, exemplified by Visual Programming (Gupta & Kembhavi, 2023), aligns with in-context learning goals by emphasizing visual task synthesis. ViperGPT (Surís et al., 2023) further demonstrates foundational models for visual reasoning, employing computational techniques similar to our objectives, though without relying on programmatic inputs. These collective efforts pave the way for more sophisticated and versatile visual in-context learning frameworks.

3 METHOD

3.1 UNIFIED REPRESENTATION OF WEATHER UNDERSTANDING TASKS.

Weather understanding tasks involve processing multi-source observational data (Veillette et al., 2020), such as geostationary satellites (GEOS), polar-orbiting satellites (POES), weather radars, and ground observation stations. Each task (e.g., weather forecasting, spatial and temporal super-resolution, weather image translation, and post-processing) utilizes different types of input and output data. To

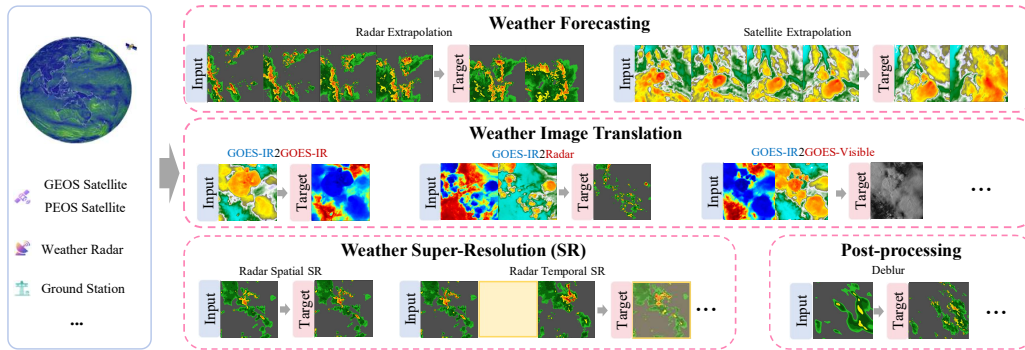


Figure 1: Illustration of the unified representation for weather understanding tasks.

address this challenge, we first developed a unified data representation that can standardize these diverse tasks. Unlike traditional methods that rely on task-specific models for each distinct task, we introduce a universal foundational model capable of addressing various weather understanding tasks through a single and general solution.

As shown in Figure 1, several key weather understanding tasks can be framed using different types of input and output data. For instance, the weather spatial super-resolution (SR) task generates a high-resolution image x_{HR} from a low-resolution image x_{LR} , while weather temporal super-resolution predicts a high-resolution image x_{HR}^t based on two consecutive observed input images x_{LR}^{t-1} and x_{LR}^t . Weather forecasting relies on a sequence of observed data points $\{x^1, x^2, \dots, x^t\}$ to predict future data points $\{x^{t+1}, x^{t+2}, \dots\}$. The image translation task focuses on converting an input image from one modality (e.g., satellite image) to another modality (e.g., radar image). Formally, we can represent these tasks as projections from the source input data X_S to the target output data X_T :

$$\tau : X_S \rightarrow X_T. \quad (1)$$

When $X_S = x_{LR}$ and $X_T = x_{HR}$, the task corresponds to spatial SR. Similarly, when $X_S = \{x^1, x^2, \dots, x^t\}$ and $X_T = \{x^{t+1}, x^{t+2}, \dots\}$, the task represents weather forecasting. As these tasks differ in their input and output formats, as well as sequence lengths, the key challenge lies in unifying them within one coherent data representation.

3.2 WEATHERGFM: WEATHER GENERALIST FOUNDATION MODEL

We present the Weather Generalist Foundation Model (WeatherGFM) to tackle the challenges inherent in a range of weather understanding tasks. Through in-context learning, our WeatherGFM can uniformly handle various weather understanding tasks involving multiple data modalities.

Weather prompt designing. In large language models and vision foundation models, task prompts commonly provide specific task-related input-output pairs. As shown in Figure 2, in machine translation (Stahlberg, 2020), the model is given English to French text pairs as prompts. The model can perform machine translation tasks based on these sample prompts for a given input. In visual tasks (Wang et al., 2023a), the visual prompt image1 may be a natural image, and image2 is the corresponding segmented image. The model will conduct the segmentation task for a new input image3 to obtain the segmented image.

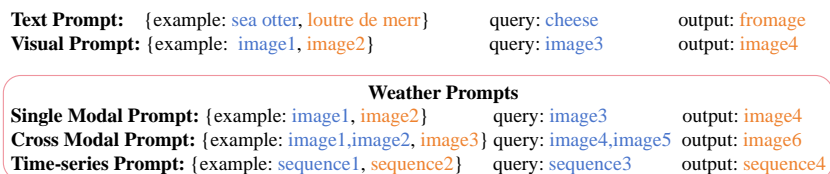


Figure 2: Comparison of weather prompts with text and visual prompts design.

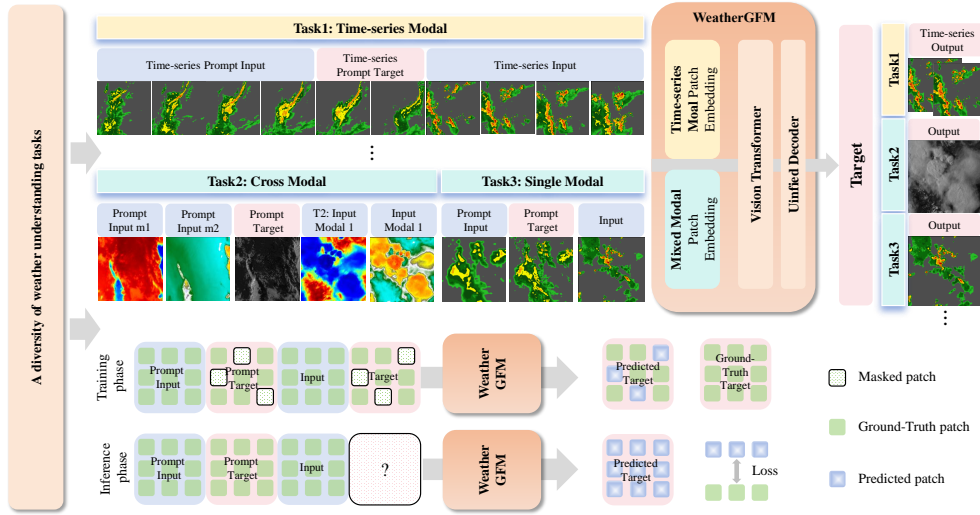


Figure 3: Overall approach of our weather generalist foundation model (WeatherGFM).

Following this paradigm, we designed weather prompts for weather understanding tasks. Since the input for weather understanding tasks involves multiple modalities, such as a single weather observation variable, multiple different weather variables, and time-series weather variables, we proposed three prompts to handle different modalities of input. In Figure 2, weather prompt1 is similar to visual prompts, converting a single modality image into a target image. In weather prompt2, the input modality can be two different channel satellite observation images (e.g., IR069 and IR107 data), and the output can be weather radar observation data for image translation tasks. In weather prompt3, time-series prompts can be input to perform weather forecasting-related tasks. With these forms of prompt design, our method can handle most weather understanding tasks.

Weather in-context learning. Inspired by the success of in-context learning in large language models (Dong et al., 2022) and vision foundation models (Wang et al., 2023a), we propose to unify the weather understanding problem as the visual prompting question-answer paradigm, as illustrated in Eq. 2. Specifically, given a visual question-answer prompt pair (P_{in}, P_{out}) as a task-guided prompt and a query input X_{in} , the model is expected to perceive the context of the prompt (i.e., what task it represents). Consequently, the model can perform the corresponding operations on the query with the prompt. This process can be formulated as follows:

$$X_{out} = F_{\tau}(X_{in}, P_{in}, P_{out}; \theta); \quad (2)$$

where F_{τ} represents a universal foundation model parameterized by θ . We can determine what task will be performed on the query sample by selecting the task-specific prompt.

Mixed-modal mask modeling. Upon redefining the output spaces of the aforementioned representative vision tasks, it is observed that both the input and output of these tasks are in the form of images as transformers-based architectures could provide flexibility by treating the image-like data as a set of tokens. Therefore, we build the WeatherGFM architecture on Vision Transformers (ViT) and propose a mixed-modal masked image modeling (MMIM) pipeline to train multiple weather understanding tasks as shown in Figure 3. Our WeatherGFM comprises three main elements: the format for input data, the architectural design, and loss function.

Input format: Given an input of shape (C, H, W) , ViT predicts an output of shape (C', H', W') , where C represents the input channels and C' represents the output channels. As shown in Figure 3, different tasks have different channels. The model tokenizes the input into a sequence of patches, with each patch having a size of $C \times p^2$, where p is the patch size. Unlike RGB-based image data, where the channels are fixed, the number of physical variables in climate and weather data can vary between different datasets and tasks. To adapt the ViT to different weather-related downstream tasks, we designed task-specific patch embedding layers within the architecture. After the patch embedding

layer, we use an MLP layer to align the embeddings of different tasks to the same space:

$$\begin{aligned} z_C &= \text{PatchEmbed}_C(x), x \in \mathbb{R}^{C \times H \times W}, \quad z_C \in \mathbb{R}^{N \times D}, \\ z_0 &= \text{MLP}_C(\text{LN}(z_C)), \quad z_0 \in \mathbb{R}^{N \times D} \end{aligned} \quad (3)$$

where N, D denotes the number of input tokens and the transformer dimension, respectively. For the masked area, we follow previous works (Liu et al., 2023a) to use a learnable token vector to replace each masked patch. We adopt the block-wise masking strategy, taking the masking ratio as 75%.

Architecture: A vanilla vision Transformer (ViT) is adopted as the backbone architecture. It consists of task-specific patch-embedded layers and several alternating layers made of Multi-Head Self-Attention (MHSA) and MLP blocks. Layer Normalization (LN) is applied before every block, and residual connections are applied after every block. As shown in Figure 3, this process can be formulated as follows:

$$\begin{aligned} z'_\ell &= \text{MHSA}(\text{LN}(z_{\ell-1})) + z_{\ell-1}, \ell = 1 \dots L, \\ z_\ell &= \text{MLP}(\text{LN}(z'_\ell)) + z'_\ell, \ell = 1 \dots L, \end{aligned} \quad (4)$$

where L denotes the number of layers. After the attention layers, we employ a prediction head and then unpatchify the output of the prediction head. The prediction head is a one-layer MLP with a hidden dimension of 1024.

Loss Function: After generate the output X_{out} , optimization objectives are as follows:

$$L_\theta(X_{out}, X_T) = \|X_{out} - X_T\|^2. \quad (5)$$

where we use MSE (mean square error) loss to train the weather generalist foundation model.

4 EXPERIMENTS

4.1 WEATHER UNDERSTANDING TASKS.

To show the versatility of our proposed method, we incorporate up to 10 tasks including diverse weather forecasting, weather super-resolution, weather image translation and weather post-processing tasks into our experiments.

SEVIR. The Storm EVent ImageRy dataset (SEVIR) (Veillette et al., 2020) is a spatiotemporally aligned dataset that contains over 10,000 weather events represented by five spatially and temporally aligned sensors. These sensors consist of three channels (C02, C09, C13) from the GOES-16 satellite, one NEXRAD derived vertically integrated liquid (VIL) mosaics variable, and lighting detections from the GOES GLM sensor. Each SEVIR event spans 4 hours with 5-minute intervals, sampled randomly (with oversampling of events with moderate and high precipitation) using the NOAA Storm Event Database. The SEVIR benchmark supports scientific research on multiple meteorological applications, including future prediction, image-to-image translation, super-resolution, etc. A detailed description of these tasks can be found in Appendix A. In our task, given that the WeatherGFM has the ability to generate images of diverse modalities, we uniformly sample the resolution of images from different modalities to 256×256 . Moreover, we perform filtering on the events within the SEVIR dataset and pick out those events that include both the three channels of the GOES-16 satellite and the one variable derived from weather radar. Ultimately, the dataset we utilize comprises 11,508 events with four distinct sensing modalities. Among them, 11,308 events are selected as the training set, while 100 events are designated as the validation set and 100 events are designated as the test set. Each SEVIR event covers a period of 4 hours with increments of 5 minutes, which implies that there are 49 images for each modality within a single event. Consequently, the training set contains a total of 2.2M images, while the validate/test set has a total of 19.6K images. Regarding the demarcation of the training set and the test set for each task, we provide a detailed introduction in Appendix A.

POMINO-TROPOMI, GEOS-CF. In addition, we add a weather image translation task for environment monitoring: Translate geostationary NO_2 data to polar-orbiting satellites NO_2 data (GEOS2POES- NO_2) based on POMINO-TROPOMI product (Liu et al., 2020) and GEOS-CF dataset (Keller et al., 2021). In this task, the input images are sourced from GEMS as well as the GEOS-CF datasets, while the output images are obtained from the TROPOMI dataset. The original image has a resolution of 1400×800 . We also divide it into grids of 256×256 with a sliding step size

Table 2: Quantitative results on weather understanding tasks. #: single-task model. †: trained with all ten weather understanding tasks. RMSE and CSI are calculated as the quantitative metric. A lower RMSE and a higher CSI indicate better results. The best results are highlighted in bold, and the second-best results are underscored.

| Task name | Weather super-resolution (SR) | | | | | | | | | | |
|-------------------------|-------------------------------|--------------|--------------|-------------------|--------------|--------------|--------------|------------------|--------------|--------------|--------------|
| | Satellite Spatial SR | | | Radar Temporal SR | | | | Radar Spatial SR | | | |
| | RMSE | CSI/-4000 | CSI/-6000 | RMSE | CSI/74 | CSI/160 | CSI/219 | RMSE | CSI/74 | CSI/160 | CSI/219 |
| UNet [#] | 0.932 | 0.650 | 0.912 | 0.739 | 0.485 | 0.182 | 0.034 | 0.650 | 0.675 | 0.400 | 0.184 |
| ViT [#] | 0.047 | <u>0.987</u> | <u>0.990</u> | <u>0.333</u> | <u>0.591</u> | <u>0.285</u> | <u>0.061</u> | 0.120 | <u>0.830</u> | <u>0.637</u> | <u>0.358</u> |
| WeatherGFM [†] | 0.042 | 0.988 | 0.996 | 0.327 | 0.597 | 0.287 | 0.073 | <u>0.121</u> | 0.831 | 0.644 | 0.375 |

| Task name | Weather Forecasting | | | | | | | Post-processing | | | |
|-------------------------|-------------------------|--------------|--------------|---------------------|--------------|--------------|--------------|-----------------|--------------|--------------|--------------|
| | Satellite extrapolation | | | Radar extrapolation | | | | Deblur | | | |
| | RMSE | CSI/-4000 | CSI/-6000 | RMSE | CSI/74 | CSI/160 | CSI/219 | RMSE | CSI/74 | CSI/160 | CSI/219 |
| UNet [#] | 1.033 | 0.617 | 0.900 | 0.815 | 0.353 | <u>0.082</u> | <u>0.007</u> | 0.713 | 0.457 | 0.145 | 0.027 |
| ViT [#] | 0.408 | <u>0.840</u> | <u>0.943</u> | <u>0.490</u> | <u>0.440</u> | 0.079 | <u>0.007</u> | 0.163 | <u>0.594</u> | 0.291 | 0.104 |
| WeatherGFM [†] | 0.347 | 0.863 | 0.951 | 0.467 | 0.465 | 0.128 | 0.021 | <u>0.264</u> | 0.629 | <u>0.255</u> | <u>0.082</u> |

| Task name | Weather image translation | | | | | | | | | | |
|-------------------------|---------------------------|--------------|--------------|--------------|--------------|--------------|-----------------|--------------|--------------|--------------|--------------|
| | GOES2Radar | | | | | | GOES-IR2GOES-IR | | | | |
| | RMSE | CSI/16 | CSI/74 | CSI/160 | CSI/181 | CSI/219 | RMSE | CSI/-6000 | CSI/-4000 | CSI/0 | CSI/2000 |
| UNet [#] | 0.821 | 0.222 | 0.370 | <u>0.180</u> | <u>0.153</u> | 0.079 | 0.915 | 0.929 | 0.741 | 0.638 | 0.078 |
| ViT [#] | 0.445 | <u>0.602</u> | <u>0.436</u> | <u>0.180</u> | 0.131 | <u>0.042</u> | 0.257 | <u>0.987</u> | 0.972 | 0.809 | <u>0.136</u> |
| WeatherGFM [†] | 0.436 | 0.619 | 0.447 | 0.208 | 0.157 | 0.053 | <u>0.310</u> | 0.993 | <u>0.968</u> | <u>0.808</u> | 0.222 |

| Task name | GOES-IR2GOES-Visible | | | | | | GOES2POES-NO ₂ | | | | |
|-------------------------|----------------------|--------------|--------------|--------------|--------------|--------------|---------------------------|--------------|--------------|--------------|--------------|
| | RMSE | CSI/2000 | CSI/3200 | CSI/4400 | CSI/5600 | CSI/6800 | RMSE | CSI/1 | CSI/5 | CSI/10 | CSI/15 |
| | UNet [#] | 0.915 | 0.422 | 0.285 | 0.179 | 0.100 | 0.040 | 0.866 | <u>0.799</u> | 0.360 | 0.274 |
| ViT [#] | 0.448 | <u>0.574</u> | <u>0.437</u> | 0.303 | 0.184 | 0.071 | 0.549 | 0.841 | <u>0.432</u> | <u>0.328</u> | 0.253 |
| WeatherGFM [†] | 0.439 | 0.580 | 0.439 | <u>0.298</u> | <u>0.166</u> | <u>0.068</u> | 0.302 | 0.682 | 0.562 | 0.382 | 0.197 |

of 128. Each original image can thus be segmented into 45 pieces of 256×256 pictures. We utilize the observational data from January 2021 to April 2022. After processing, each modality has 20,000 images with a resolution of 256×256. Among them, we allocate 18,000 images as the training set, 1,000 images as the validation set, and 1,000 images as the test set.

4.2 IMPLEMENTATION AND EVALUATION

Training details. During training, we resize the weather images of different resolutions to a resolution of 256×256 and input them into the model in accordance with the combination mode of $P_{in}, P_{out}, X_{in}, X_{out}$ in the task-specific prompt format, resulting in a $N \times 256 \times 256$ total input resolution. The L1 loss is employed as the loss function. For optimization, the AdamW optimizer with a cosine learning rate scheduler is utilized. The base learning rate is 1e4. The batch size is 20.

Evaluation metrics. Besides RMSE, we also include the Critical Success Index (CSI), which is commonly used in weather understanding tasks (e.g., precipitation nowcasting) and is defined as

$$CSI = \frac{\text{Hits}}{\text{Hits} + \text{Misses} + \text{F.Alarms}}$$

To count the Hits (truth=1, pred=1), Misses (truth=1, pred=0) and F.Alarms (truth=0, pred=1), the prediction and the ground-truth are normalized using mean-variance normalization and binarized at different thresholds. For radar output tasks, we have established thresholds at [16, 74, 133, 160, 181, 219]. GEOS-visible output tasks are assigned thresholds of [2000, 3200, 4400, 5600, 6800]. The GEOS-IR107 output tasks operate with thresholds set to [-6000, -4000, 0, 2000]. Lastly, the GEOS-IR069 output task employs thresholds of [-4000, -5000, -6000, -7000].

Table 3: Standard deviation of the performance computed based on 20 different prompts. Avg. CSI denotes the mean of the CSI score across thresholds [16, 74, 133, 160, 181, 219].

| | GOES2Radar | Radar extrapolation | GOES-IR2GOES-IR | Radar Spatial SR | Radar Temporal SR | Deblur |
|-----------|------------|---------------------|-----------------|------------------|-------------------|--------|
| Avg. RMSE | 0.0087 | 0.0012 | 0.0481 | 0.0001 | 0.0002 | 0.0016 |
| Avg. CSI | 0.0187 | 0.0201 | 0.0284 | 0.0006 | 0.0010 | 0.0047 |

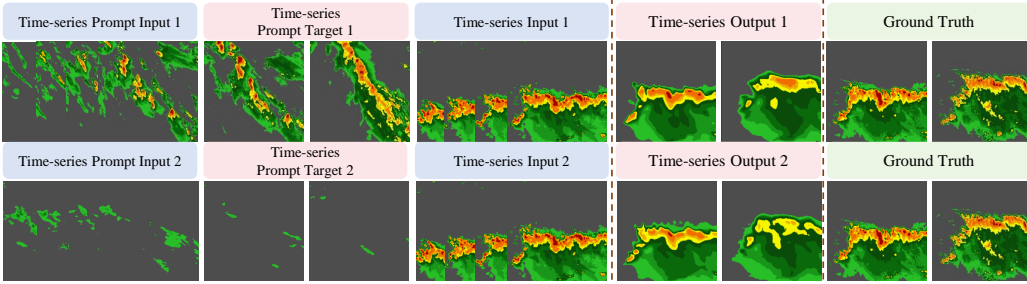


Figure 4: Case studies of our WeatherGFM with different prompts in the radar extrapolation task.

4.3 EXPERIMENTAL RESULTS

Currently, there is no general weather foundation model that can comprehensively handle all the discussed weather understanding tasks simultaneously. Although many machine learning methods have been investigated for single tasks, they generally adopt different backbone networks and design strategies tailored to them. For a fair comparison, we have trained a series of baselines (i.e., single-task model) for each weather understanding task under a consistent training setup, including commonly used UNet (Trebing et al., 2021) and ViT (Nguyen et al., 2023) networks. Notably, the purpose of this paper is not to achieve state-of-the-art performance on every task. We focus on examining whether a generalist foundation model can handle multiple complex weather understanding tasks and weather data modalities. Beyond quantitative performance results, we are more concerned with the prompt learning capabilities of the generalist foundation model and the generalization ability it brings.

Weather generalist foundation model can achieve strong universal capabilities. As seen in Table 2, our WeatherGFM, equipped with a straightforward ViT backbone, shows impressive performance and adaptability in ten weather understanding tasks. It is not only capable of conducting weather forecasting and super-resolution tasks but is also proficient in dealing with weather image translation and post-processing tasks. Overall, our WeatherGFM achieves promising performance on a diversity of weather understanding tasks.

Weather generalist foundation model outperforms the performance of the single-task model. In Table 2, we notice that our WeatherGFM achieves results that outperform the baseline in weather forecasting, weather super-resolution, and image translation tasks. For instance, in radar extrapolation tasks, our WeatherGFM with universal ViT-based model outperforms the single-task ViT model. This indicates that a unified approach to weather understanding tasks can potentially break the performance upperbound of single-task models.

In-context learning can generate correct outputs across a variety of data modalities and tasks. As depicted in Figure 5, our WeatherGFM effectively carries out a wide array of weather understanding tasks on multi-modal weather data. In practical scenarios, weather forecasting and weather image transformation represent two substantially different tasks due to differences in temporal modalities. Despite their intricacies, our WeatherGFM with in-context learning can successfully recognize distinct task types, highlighting its significant generalization capacity.

4.4 ABLATION STUDIES AND EXPLORATIONS

Exploration of different task prompts. To investigate the impact of various visual prompts on quantitative performance, we randomly select 20 meteorological prompts for each task and calculate their quantitative metrics on the test set. Table 3 presents the standard deviation of performance for

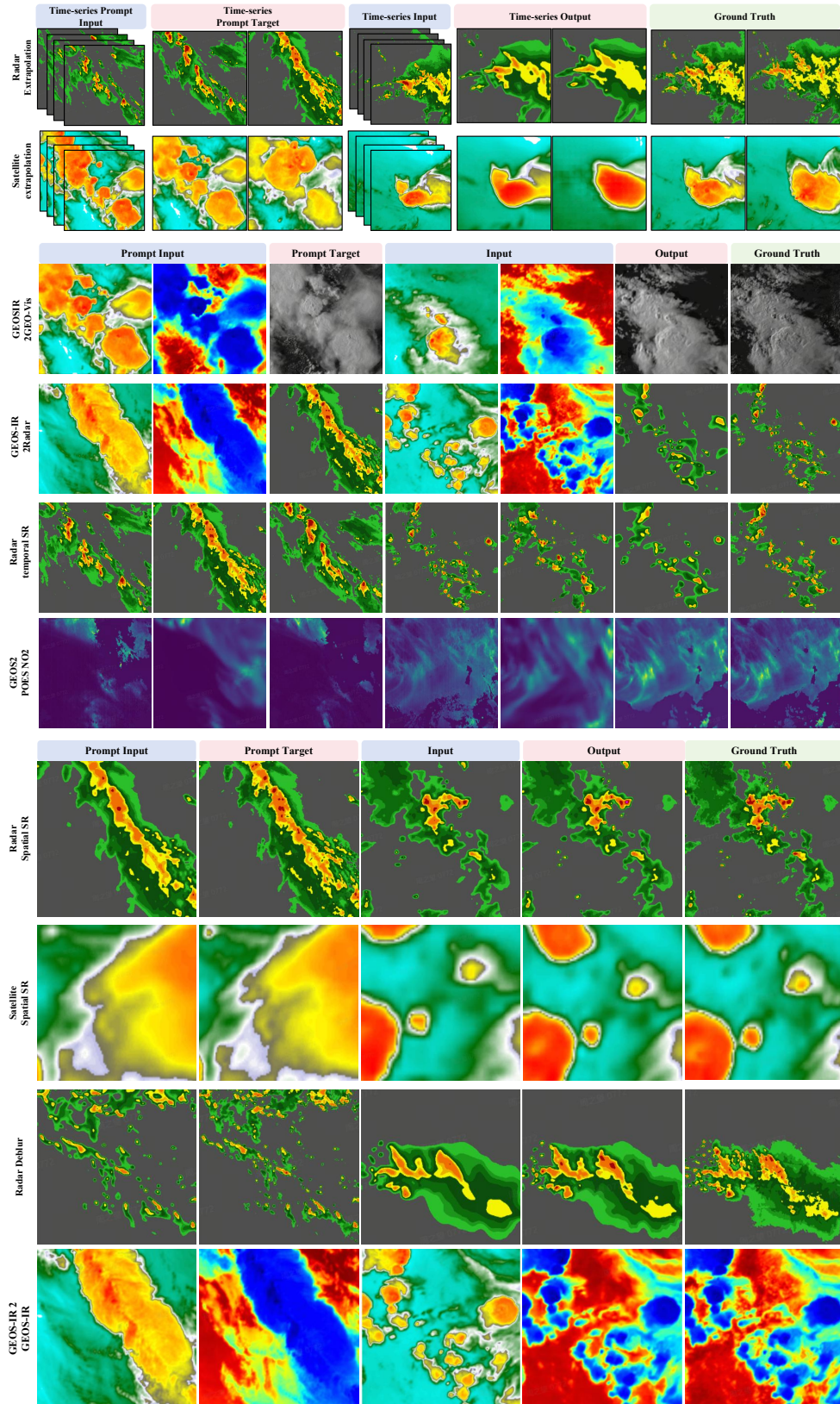


Figure 5: Visual results of the weather understanding tasks by our WeatherGFM.

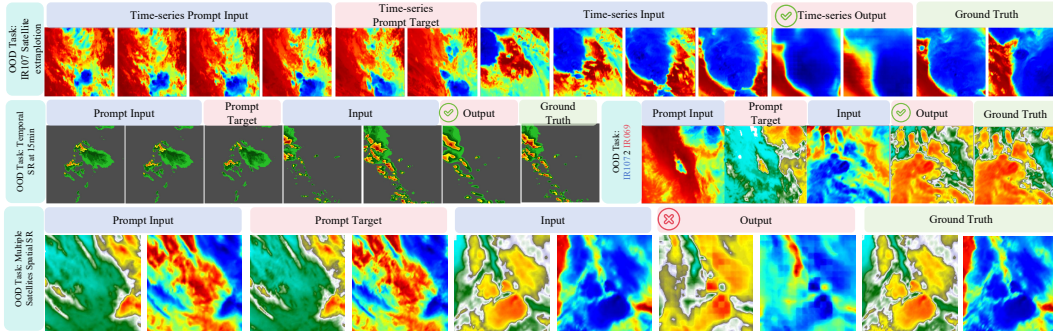


Figure 6: Visual results of our our WeatherGFM on OOD tasks.

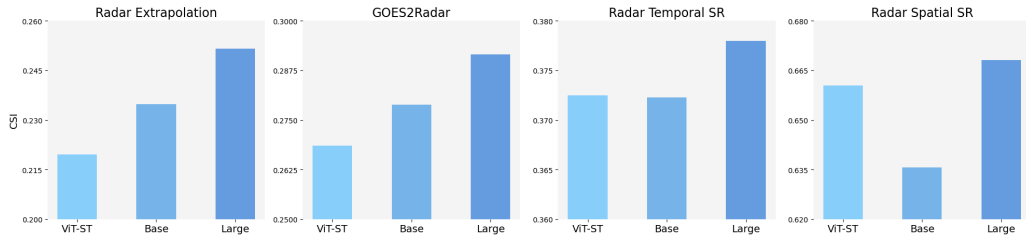


Figure 7: The effect of dataset size and model sizes. ViT-ST: single-task ViT trained on 0.5 million samples. Base: our WeatherGFM with 100 M parameters trained on 4 million samples. Large: our WeatherGFM with 330 M parameters trained on 4 million samples.

each task across the 20 distinct meteorological prompts. We note that weather super-resolution tasks are minimally affected by the randomness of weather prompts, whereas weather forecasting tasks and image transformation tasks exhibit more significant variability, reaching approximately 0.02 in CSI. Figure 4 illustrates that for certain weather events, employing different prompts yields more precise outputs. This indicates that our method can comprehend specific weather cases based on weather prompts rather than being a black box model incapable of interactive operations.

Exploration on out-of-distribution tasks. To evaluate the generalization ability of our WeatherGFM, we have devised a variety of out-of-distribution (OOD) tasks that were not encountered during the training phase, including GEOS-IR107 extrapolation, weather image translation GEOS-IR107 to GEOS-IR069, weather temporal SR at 15 minutes and GEOS-visible satellite extrapolation. As shown in Figure 6, our WeatherGFM generates correct outputs for the first three tasks, which are similar to the training distribution. However, the model encounters difficulties with the more challenging task of multiple-modal satellite spatial SR, where its outputs fail to provide effective meteorological information. These OOD tests demonstrate the model’s ability to identify tasks outside the training distribution from new prompts, showcasing a degree of generalization.

Scaling law of weather foundation model. To evaluate the impact of data and model scale on performance, we compared single-task models, the base version of our WeatherGFM, and its large version. We established a baseline using a 30M parameter ViT under a single-task with 0.5 million samples. Subsequently, in a multi-task setting with 4 million samples, our model was configured with a base version of 110M and a large version of 330M parameters. Figure 7 illustrates that improvements in performance on various tasks are achieved with the increase of model and data scale. In SR task, we observe that scaling up both the data and the model is essential for performance gains.

5 CONCLUSION

We introduce the first weather generalist foundation model, WeatherGFM. By employing a unified representation for multiple weather understanding tasks and a multi-modal prompt design, our WeatherGFM skillfully addresses various tasks, such as weather forecasting, super-resolution, image

translation, and post-processing through in-context learning. We conduct comprehensive explorations of the model’s adaptability for various tasks and its generalization capabilities to unseen tasks, and its scaling law at the data and model size. This study will facilitate the development of future large-scale generalist weather and climate foundation models.

REFERENCES

- Kaifeng Bi, Lingxi Xie, Hengheng Zhang, Xin Chen, Xiaotao Gu, and Qi Tian. Accurate medium-range global weather forecasting with 3d neural networks. *Nature*, 619(7970):533–538, 2023a.
- Zhen Bi, Ningyu Zhang, Yida Xue, Yixin Ou, Daxiong Ji, Guozhou Zheng, and Huajun Chen. Oceanopt: A large language model for ocean science tasks. *arXiv preprint arXiv:2310.02031*, 2023b.
- Cristian Bodnar, Wessel P Bruinsma, Ana Lucic, Megan Stanley, Johannes Brandstetter, Patrick Garvan, Maik Riechert, Jonathan Weyn, Haiyu Dong, Anna Vaughan, et al. Aurora: A foundation model of the atmosphere. *arXiv preprint arXiv:2405.13063*, 2024.
- Tom B Brown. Language models are few-shot learners. *arXiv preprint arXiv:2005.14165*, 2020.
- Hanting Chen, Yunhe Wang, Tianyu Guo, Chang Xu, Yiping Deng, Zhenhua Liu, Siwei Ma, Chunjing Xu, Chao Xu, and Wen Gao. Pre-trained image processing transformer. In *Proceedings of the IEEE/CVF conference on computer vision and pattern recognition*, pp. 12299–12310, 2021.
- Kang Chen, Tao Han, Junchao Gong, Lei Bai, Fenghua Ling, Jing-Jia Luo, Xi Chen, Leiming Ma, Tianning Zhang, Rui Su, et al. Fengwu: Pushing the skillful global medium-range weather forecast beyond 10 days lead. *arXiv preprint arXiv:2304.02948*, 2023a.
- Shengchao Chen, Guodong Long, Tao Shen, and Jing Jiang. Prompt federated learning for weather forecasting: Toward foundation models on meteorological data. *arXiv preprint arXiv:2301.09152*, 2023b.
- Shengchao Chen, Guodong Long, Tao Shen, Tianyi Zhou, and Jing Jiang. Spatial-temporal prompt learning for federated weather forecasting. *arXiv preprint arXiv:2305.14244*, 2023c.
- Xiangyu Chen, Xintao Wang, Wenlong Zhang, Xiangtao Kong, Yu Qiao, Jiantao Zhou, and Chao Dong. Hat: Hybrid attention transformer for image restoration. *arXiv preprint arXiv:2309.05239*, 2023d.
- Xiangyu Chen, Yihao Liu, Yuandong Pu, Wenlong Zhang, Jiantao Zhou, Yu Qiao, and Chao Dong. Learning a low-level vision generalist via visual task prompt. *arXiv preprint arXiv:2408.08601*, 2024a.
- Xiangyu Chen, Yihao Liu, Yuandong Pu, Wenlong Zhang, Jiantao Zhou, Yu Qiao, and Chao Dong. Learning a low-level vision generalist via visual task prompt. *arXiv preprint arXiv:2408.08601*, 2024b.
- Xuanhong Chen, Kairui Feng, Naiyuan Liu, Bingbing Ni, Yifan Lu, Zhengyan Tong, and Ziang Liu. Rainnet: A large-scale imagery dataset and benchmark for spatial precipitation downscaling. *Advances in Neural Information Processing Systems*, 35:9797–9812, 2022.
- Qingxiu Dong, Lei Li, Damai Dai, Ce Zheng, Zhiyong Wu, Baobao Chang, Xu Sun, Jingjing Xu, and Zhifang Sui. A survey on in-context learning. *arXiv preprint arXiv:2301.00234*, 2022.
- Yujie Feng, Zexin Lu, Bo Liu, Liming Zhan, and Xiao-Ming Wu. Towards llm-driven dialogue state tracking. *arXiv preprint arXiv:2310.14970*, 2023.
- Zhihan Gao, Xingjian Shi, Boran Han, Hao Wang, Xiaoyong Jin, Danielle Maddix, Yi Zhu, Mu Li, and Yuyang Bernie Wang. Prediff: Precipitation nowcasting with latent diffusion models. *Advances in Neural Information Processing Systems*, 36, 2024.
- Junchao Gong, Lei Bai, Peng Ye, Wanghan Xu, Na Liu, Jianhua Dai, Xiaokang Yang, and Wanli Ouyang. Cascast: Skillful high-resolution precipitation nowcasting via cascaded modelling. *arXiv preprint arXiv:2402.04290*, 2024a.

-
- Junchao Gong, Siwei Tu, Weidong Yang, Ben Fei, Kun Chen, Wenlong Zhang, Xiaokang Yang, Wanli Ouyang, and Lei Bai. Postcast: Generalizable postprocessing for precipitation nowcasting via unsupervised blurriness modeling. *arXiv preprint arXiv:2410.05805*, 2024b.
- Tanmay Gupta and Aniruddha Kembhavi. Visual programming: Compositional visual reasoning without training. In *Proceedings of the IEEE/CVF Conference on Computer Vision and Pattern Recognition*, pp. 14953–14962, 2023.
- Tao Han, Song Guo, Fenghua Ling, Kang Chen, Junchao Gong, Jingjia Luo, Junxia Gu, Kan Dai, Wanli Ouyang, and Lei Bai. Fengwu-ghr: Learning the kilometer-scale medium-range global weather forecasting. *arXiv preprint arXiv:2402.00059*, 2024.
- Hans Hersbach, Bill Bell, Paul Berrisford, Shoji Hirahara, András Horányi, Joaquín Muñoz-Sabater, Julien Nicolas, Carole Peubey, Raluca Radu, Dinand Schepers, et al. The era5 global reanalysis. *Quarterly Journal of the Royal Meteorological Society*, 146(730):1999–2049, 2020.
- Alberto Hojel, Yutong Bai, Trevor Darrell, Amir Globerson, and Amir Bar. Finding visual task vectors. *arXiv preprint arXiv:2404.05729*, 2024.
- Weidong Hu, Wenlong Zhang, Shi Chen, Xin Lv, Dawei An, and Leo Ligthart. A deconvolution technology of microwave radiometer data using convolutional neural networks. *Remote Sensing*, 10(2):275, 2018.
- Weidong Hu, Yade Li, Wenlong Zhang, Shi Chen, Xin Lv, and Leo Ligthart. Spatial resolution enhancement of satellite microwave radiometer data with deep residual convolutional neural network. *Remote Sensing*, 11(7):771, 2019.
- Langwen Huang, Lukas Gianinazzi, Yuejiang Yu, Peter D Dueben, and Torsten Hoefler. Diffda: a diffusion model for weather-scale data assimilation. *arXiv preprint arXiv:2401.05932*, 2024.
- Christoph A Keller, K Emma Knowland, Bryan N Duncan, Junhua Liu, Daniel C Anderson, Sampa Das, Robert A Lucchesi, Elizabeth W Lundgren, Julie M Nicely, Eric Nielsen, et al. Description of the nasa geos composition forecast modeling system geos-cf v1. 0. *Journal of Advances in Modeling Earth Systems*, 13(4):e2020MS002413, 2021.
- Yade Li, Weidong Hu, Shi Chen, Wenlong Zhang, Rui Guo, Jingwen He, and Leo Ligthart. Spatial resolution matching of microwave radiometer data with convolutional neural network. *Remote Sensing*, 11(20):2432, 2019.
- Fenghua Ling, Zeyu Lu, Jing-Jia Luo, Lei Bai, Swadhin K Behera, Dachao Jin, Baoxiang Pan, Huidong Jiang, and Toshio Yamagata. Diffusion model-based probabilistic downscaling for 180-year east asian climate reconstruction. *npj Climate and Atmospheric Science*, 7(1):131, 2024.
- Haotian Liu, Chunyuan Li, Qingyang Wu, and Yong Jae Lee. Visual instruction tuning. *Advances in neural information processing systems*, 36, 2024a.
- Mengyao Liu, Jintai Lin, Hao Kong, K Folkert Boersma, Henk Eskes, Yugo Kanaya, Qin He, Xin Tian, Kai Qin, Pinhua Xie, et al. A new tropomi product for tropospheric no 2 columns over east asia with explicit aerosol corrections. *Atmospheric Measurement Techniques*, 13(8):4247–4259, 2020.
- Qijiong Liu, Jieming Zhu, Yanting Yang, Quanyu Dai, Zhaocheng Du, Xiao-Ming Wu, Zhou Zhao, Rui Zhang, and Zhenhua Dong. Multimodal pretraining, adaptation, and generation for recommendation: A survey. In *Proceedings of the 30th ACM SIGKDD Conference on Knowledge Discovery and Data Mining*, pp. 6566–6576, 2024b.
- Yihao Liu, Xiangyu Chen, Xianzheng Ma, Xintao Wang, Jiantao Zhou, Yu Qiao, and Chao Dong. Unifying image processing as visual prompting question answering. *arXiv preprint arXiv:2310.10513*, 2023a.
- Yihao Liu, Xiangyu Chen, Xianzheng Ma, Xintao Wang, Jiantao Zhou, Yu Qiao, and Chao Dong. Unifying image processing as visual prompting question answering. *arXiv preprint arXiv:2310.10513*, 2023b.

-
- Yuanbo Liu, Qiaoni Fu, Ping Song, Xiaosong Zhao, and Cuicui Dou. Satellite retrieval of precipitation: An overview. *Advances in Earth Science*, 26(11):1162, 2011.
- Zili Liu, Hao Chen, Lei Bai, Wenyan Li, Keyan Chen, Zhengyi Wang, Wanli Ouyang, Zhengxia Zou, and Zhenwei Shi. Observation-guided meteorological field downscaling at station scale: A benchmark and a new method. *arXiv preprint arXiv:2401.11960*, 2024c.
- Jiasen Lu, Christopher Clark, Rowan Zellers, Roozbeh Mottaghi, and Aniruddha Kembhavi. Unified-io: A unified model for vision, language, and multi-modal tasks. In *The Eleventh International Conference on Learning Representations*, 2022.
- Jiasen Lu, Christopher Clark, Sangho Lee, Zichen Zhang, Savya Khosla, Ryan Marten, Derek Hoiem, and Aniruddha Kembhavi. Unified-io 2: Scaling autoregressive multimodal models with vision language audio and action. In *Proceedings of the IEEE/CVF Conference on Computer Vision and Pattern Recognition*, pp. 26439–26455, 2024.
- Xin Man, Chenghong Zhang, Jin Feng, Changyu Li, and Jie Shao. W-mae: Pre-trained weather model with masked autoencoder for multi-variable weather forecasting. *arXiv preprint arXiv:2304.08754*, 2023.
- Tung Nguyen, Johannes Brandstetter, Ashish Kapoor, Jayesh K Gupta, and Aditya Grover. Climax: A foundation model for weather and climate. *arXiv preprint arXiv:2301.10343*, 2023.
- Jaideep Pathak, Shashank Subramanian, Peter Harrington, Sanjeev Raja, Ashesh Chattopadhyay, Morteza Mardani, Thorsten Kurth, David Hall, Zongyi Li, Kamyar Azizzadenesheli, et al. Fourcast-net: A global data-driven high-resolution weather model using adaptive fourier neural operators. *arXiv preprint arXiv:2202.11214*, 2022.
- Shukla, P. B., Pal, K. P., Joshi, and C. P. Extrapolation of sequence of geostationary satellite images for weather nowcasting. *Geoscience and Remote Sensing Letters IEEE*, 2011.
- Felix Stahlberg. Neural machine translation: A review. *Journal of Artificial Intelligence Research*, 69:343–418, 2020.
- Jason Stock, Kyle Hilburn, Imme Ebert-Uphoff, and Charles Anderson. Srvit: Vision transformers for estimating radar reflectivity from satellite observations at scale. *arXiv preprint arXiv:2406.16955*, 2024.
- Dídac Surís, Sachit Menon, and Carl Vondrick. Vipergpt: Visual inference via python execution for reasoning. In *Proceedings of the IEEE/CVF International Conference on Computer Vision*, pp. 11888–11898, 2023.
- Kevin Trebing, Tomasz Stanczyk, and Siamak Mehrkanoon. Smaat-unet: Precipitation nowcasting using a small attention-unet architecture. *Pattern Recognition Letters*, 145:178–186, 2021.
- Thomas Vandal, Evan Kodra, Sangram Ganguly, Andrew Michaelis, Ramakrishna Nemani, and Auroop R Ganguly. DeepSD: Generating high resolution climate change projections through single image super-resolution. In *Proceedings of the 23rd acm sigkdd international conference on knowledge discovery and data mining*, pp. 1663–1672, 2017.
- Mark Veillette, Siddharth Samsi, and Chris Mattioli. Sevir: A storm event imagery dataset for deep learning applications in radar and satellite meteorology. *Advances in Neural Information Processing Systems*, 33:22009–22019, 2020.
- Cong Wang, Jinshan Pan, Wanyu Lin, Jiangxin Dong, Wei Wang, and Xiao-Ming Wu. Selfpromer: Self-prompt dehazing transformers with depth-consistency. In *Proceedings of the AAAI Conference on Artificial Intelligence*, volume 38, pp. 5327–5335, 2024a.
- Wuxin Wang, Weicheng Ni, Tao Han, Lei Bai, Boheng Duan, and Kaijun Ren. Dabench: A benchmark dataset for data-driven weather data assimilation. *arXiv preprint arXiv:2408.11438*, 2024b.
- Xinlong Wang, Wen Wang, Yue Cao, Chunhua Shen, and Tiejun Huang. Images speak in images: A generalist painter for in-context visual learning. In *Proceedings of the IEEE/CVF Conference on Computer Vision and Pattern Recognition*, pp. 6830–6839, 2023a.

-
- Xinlong Wang, Wen Wang, Yue Cao, Chunhua Shen, and Tiejun Huang. Images speak in images: A generalist painter for in-context visual learning. In *Proceedings of the IEEE/CVF Conference on Computer Vision and Pattern Recognition*, pp. 6830–6839, 2023b.
- Nicolas Webersinke, Mathias Kraus, Julia Anna Bingler, and Markus Leippold. Climatebert: A pretrained language model for climate-related text. *arXiv preprint arXiv:2110.12010*, 2021.
- Wanghan Xu, Fenghua Ling, Wenlong Zhang, Tao Han, Hao Chen, Wanli Ouyang, and Lei Bai. Generalizing weather forecast to fine-grained temporal scales via physics-ai hybrid modeling. *arXiv preprint arXiv:2405.13796*, 2024.
- Wenlong Zhang, Yihao Liu, Chao Dong, and Yu Qiao. Ranksrgan: Generative adversarial networks with ranker for image super-resolution. In *Proceedings of the IEEE/CVF international conference on computer vision*, pp. 3096–3105, 2019.
- Wenlong Zhang, Yihao Liu, Chao Dong, and Yu Qiao. Ranksrgan: Super resolution generative adversarial networks with learning to rank. *IEEE Transactions on Pattern Analysis and Machine Intelligence*, 44(10):7149–7166, 2021.
- Wenlong Zhang, Guangyuan Shi, Yihao Liu, Chao Dong, and Xiao-Ming Wu. A closer look at blind super-resolution: Degradation models, baselines, and performance upper bounds. In *Proceedings of the IEEE/CVF conference on computer vision and pattern recognition*, pp. 527–536, 2022.
- Wenlong Zhang, Xiaohui Li, Xiangyu Chen, Yu Qiao, Xiao-Ming Wu, and Chao Dong. Seal: A framework for systematic evaluation of real-world super-resolution. *arXiv preprint arXiv:2309.03020*, 2023.
- Wenlong Zhang, Xiaohui Li, Guangyuan Shi, Xiangyu Chen, Yu Qiao, Xiaoyun Zhang, Xiao-Ming Wu, and Chao Dong. Real-world image super-resolution as multi-task learning. *Advances in Neural Information Processing Systems*, 36, 2024.
- Xiangyu Zhao, Bo Liu, Qijiong Liu, Guangyuan Shi, and Xiao-Ming Wu. Easygen: Easing multimodal generation with bidiffuser and llms. In *Proceedings of the 62nd Annual Meeting of the Association for Computational Linguistics (Volume 1: Long Papers)*, pp. 1351–1370, 2024a.
- Xiangyu Zhao, Yuehan Zhang, Wenlong Zhang, and Xiao-Ming Wu. Unifashion: A unified vision-language model for multimodal fashion retrieval and generation. *arXiv preprint arXiv:2408.11305*, 2024b.

A DETAILS OF WEATHER UNDERSTANDING TASKS

Weather forecasting. Radar echo extrapolation aims to forecast data for the subsequent 1-2 hours utilizing observations from past moments (Gao et al., 2024). This task, similar to precipitation nowcasting, plays a significant role in predicting local weather conditions. It can directly impact traffic plans, disaster warnings, and energy management. Likewise, meteorological satellite image extrapolation is crucial for monitoring and analyzing meteorological conditions. Based on the SEVIR dataset, we consider two weather forecasting tasks: radar echo extrapolation Gong et al. (2024a) and satellite image extrapolation (Shukla et al., 2011). Our weather prediction tasks incorporate observations from the hour before (0, 30, 60, and 90 minutes past) and the hour ahead (120 and 180 minutes into the future) for both radar and satellite IR-069 extrapolation. Consequently, for this task, the SEVIR data was extracted and processed to generate 135,696 sequences for training, along with an independent set of 1,200 sequences to validate/test the fitted model.

Weather super-resolution (SR). Weather spatial super-resolution task (Veillette et al., 2020; Hu et al., 2018; 2019; Li et al., 2019) generates a high-resolution image from a low-resolution(LR) image, while temporal super-resolution predicts a high-resolution(HR) image based on two consecutive observed input images. We take into consideration three weather super-resolution tasks: spatial SR for satellite IR-069, spatial SR for radar VIL, and temporal SR for radar VIL with a one-hour interval. We utilize the SEVIR dataset as the source of the HR image. To obtain the LR image, we employ the “Bicubic” interpolation approach, which is commonly used in vision image SR (Zhang et al., 2019; 2021). In the context of meteorology, this is analogous to statistical downscaling, as described in statistical downscaling (Vandal et al., 2017). Specifically, for the VIL image, given that its original resolution is 384×384 , we resize it to 256×256 to serve as the HR image and resize it to 64×64 to function as the LR image, thereby implementing a 4x super-resolution task. For the IR-069 image, since its original image has a resolution of 196×196 , we resize it to 256×256 to be the HR image and resize it to 64×64 to be the LR image, thus carrying out a 3x super-resolution task. For each spatial SR for satellite tasks, the SEVIR data was extracted and processed to yield 542,784 images for training, along with an independent set of 4,800 images for validating/testing. For the weather temporal SR, we use the radar VIL image at 1 hour (0 and 60 minutes) as the input to predict the radar VIL image at 30 minutes. For the temporal SR task, the SEVIR data was further extracted and processed to generate 407,088 sequences for training, along with an independent set of 3,600 sequences to validate/test the fitted model.

Weather image translation. Weather image translation involves converting observation data (e.g., satellite data) to a desired weather image (Veillette et al., 2020). For example, depictions of storms obtained from weather radar are extremely important. However, most areas of the world do not have access to ground-based radar. It is useful for generating weather radar images of storm depictions from satellite observation (Veillette et al., 2020). We consider three weather image translation tasks based on SEVIR dataset: translate geostationary IR-069 to geostationary IR-107 data (GEOS-IR2GEOS-IR), geostationary IR-069 to geostationary Visible data (GEOS-IR2GEOS-Vis), translate geostationary IR-069 and IR-107 to radar VIL data (GEOS-IR2Radar). In addition, we add a weather image translation task for environment monitoring: Translate geostationary NO_2 data to polar-orbiting satellites NO_2 data (GEOS2POES- NO_2) based on POMINO-TROPOMI (Liu et al., 2020) and GEOS-CF (Keller et al., 2021) product. For the image translation tasks based on SEVIR dataset, we split SEVIR into 542,784 training samples, 4,800 validation samples and 4,800 test samples. For translating geostationary NO_2 data, the input images are sourced from GEMS as well as the GEOS-CF datasets, while the output images are obtained from the TROPOMI dataset. Each modality has 20,000 images with a resolution of 256×256 . Among them, we allocate 18,000 images as the training set, 1,000 images as the validation set, and 1,000 images as the test set.

Weather post-processing: Post-processing (e.g., bias correction) aims to minimize or eliminate systematic biases in model outputs and observational data, which emerge due to uncertainties in weather models and measurement errors. Various methods, including statistical, machine learning, and deep learning techniques, can be employed for post-processing, tailoring the approach based on the specific application and data characteristics. By minimizing or eliminating systematic biases, post-processing improves the quality and reliability of weather and climate data. In our experiment, we consider a classic post-processing task: Deblurring for radar VIL nowcasting. We employ the output of Earthformer and the corresponding high-quality image as a training sample. Deblurring aims to learn how to map from the output of Earthformer to the corresponding high-quality image.

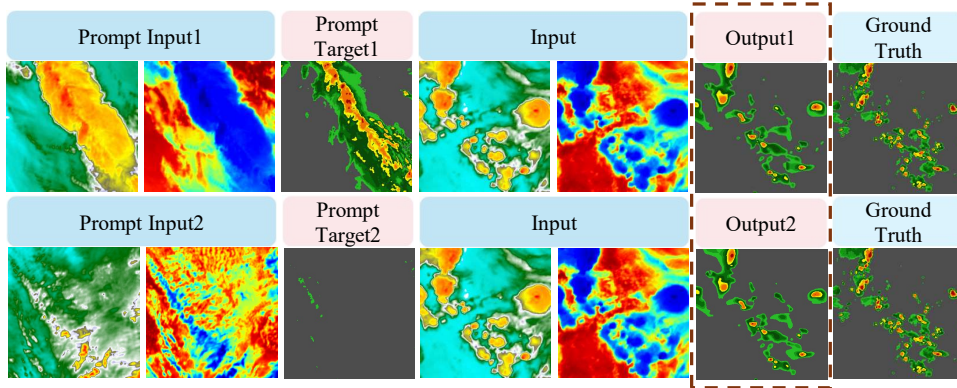


Figure 8: Case studies of our WeatherGFM with different prompts in GEOS-IR2Radar task.

Table 4: Comparison of the models with random prompts, high-quality prompts, and searched prompts according to RMSE.

| Tasks | GOES2Radar | | | | | Radar Extrapolation | | | | |
|------------------|------------|---------|---------|---------|---------|---------------------|---------|---------|---------|---------|
| | CSI/74 | CSI/133 | CSI/160 | CSI/181 | CSI/219 | CSI/74 | CSI/133 | CSI/160 | CSI/181 | CSI/219 |
| random prompts | 0.389 | 0.238 | 0.194 | 0.15 | 0.048 | 0.423 | 0.187 | 0.106 | 0.069 | 0.017 |
| high prompts | 0.399 | 0.249 | 0.208 | 0.164 | 0.057 | 0.426 | 0.191 | 0.11 | 0.072 | 0.019 |
| searched prompts | 0.401 | 0.24 | 0.199 | 0.155 | 0.049 | 0.425 | 0.188 | 0.108 | 0.071 | 0.018 |

B EFFECTS OF VISUAL PROMPTS

To assess the effectiveness of visual prompts within the WeatherGFM framework, we conducted a series of tests across various scenarios, including GOES2Radar, Radar Extrapolation, GOES-IR2GOES-IR, Radar Spatial SR, Radar Temporal SR, and Deblur tasks. In our main paper, we detail a thorough process of prompt selection, curating 20 unique prompts for each task and subsequently reporting the most favorable quantitative outcomes. The comprehensive results of these prompt variations on several representative tasks are presented in the tables.

By examining Table 5, we observed that prompts have a significant impact on the GOES2Radar and Radar Extrapolation tasks. Consequently, we conducted further experiments on these two tasks. The results are shown in Table 4. In these experiments, “random prompt” refers to prompts selected randomly, while “high prompt” refers to prompts selected from a high-quality prompt base derived from radar data. Specifically, we grouped 100 events and selected samples that contained values exceeding a threshold of 50 within each group, totaling 113 samples. Prompts were then randomly selected from this high-quality base for the experiments. “Searched prompt” refers to a method where prompts are selected based on the RMSE metric calculated from the input images to find similar prompts.

C MORE DETAILS OF SCALING LAW

In Figure 9, we present the results of the RMSE metric that compares single-task models, the base version of our WeatherGFM, and its large version. It can be observed that increasing the capacity of the model generally leads to better performance when the data size remains constant. In contrast, for smaller models, an increase in training data may result in poorer performance. We hypothesize that this could be due to the specificity of different tasks within the training data, which makes it more challenging for the model to fit effectively.

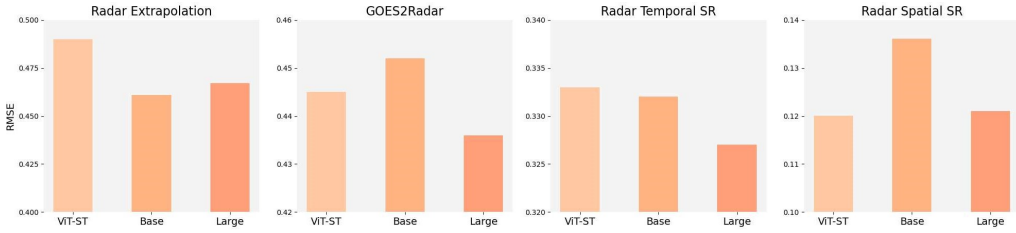


Figure 9: RMSE performance comparison across different model configurations.

Table 5: Influence of employing different visual prompts on different tasks. The color red is used for the poorest-performing prompts, and green is used for the best-performing prompts.

| Prompts | | Idx0 | Idx1 | Idx2 | Idx3 | Idx4 | Idx5 | Idx6 | Idx7 | Idx8 | Idx9 |
|---------------------|------|--------|--------|--------|--------|--------|--------|--------|--------|--------|--------|
| GOES2Radar | RMSE | 0.4759 | 0.471 | 0.5117 | 0.4748 | 0.4691 | 0.4725 | 0.4726 | 0.4692 | 0.4722 | 0.473 |
| | CSI | 0.3401 | 0.3335 | 0.3233 | 0.3300 | 0.3452 | 0.3298 | 0.3272 | 0.2467 | 0.3302 | 0.3317 |
| Radar Extrapolation | RMSE | 0.4912 | 0.4908 | 0.4891 | 0.4925 | 0.4933 | 0.4937 | 0.4933 | 0.493 | 0.4933 | 0.4951 |
| | CSI | 0.3401 | 0.2497 | 0.2534 | 0.2479 | 0.2484 | 0.2467 | 0.2462 | 0.2467 | 0.2453 | 0.2467 |
| GOES-IR2GOES-IR | RMSE | 0.283 | 0.2947 | 0.2593 | 0.3791 | 0.2424 | 0.2989 | 0.3213 | 0.2811 | 0.4372 | 0.387 |
| | CSI | 0.6851 | 0.6907 | 0.6963 | 0.6559 | 0.6958 | 0.7525 | 0.6835 | 0.7314 | 0.6240 | 0.6529 |
| Radar Spatial SR | RMSE | 0.1331 | 0.1331 | 0.1334 | 0.1331 | 0.1332 | 0.1335 | 0.1334 | 0.1333 | 0.1333 | 0.1335 |
| | CSI | 0.7208 | 0.7206 | 0.7209 | 0.7208 | 0.7228 | 0.7222 | 0.7221 | 0.7227 | 0.7217 | 0.7225 |
| Radar Temporal SR | RMSE | 0.3166 | 0.3166 | 0.3164 | 0.3164 | 0.3168 | 0.3172 | 0.3168 | 0.3166 | 0.317 | 0.3172 |
| | CSI | 0.3387 | 0.3395 | 0.3389 | 0.3359 | 0.3398 | 0.3366 | 0.3376 | 0.3376 | 0.3372 | 0.3388 |
| Deblur | RMSE | 0.2272 | 0.2236 | 0.2236 | 0.2255 | 0.2253 | 0.2274 | 0.2273 | 0.2286 | 0.2241 | 0.2233 |
| | CSI | 0.3412 | 0.3405 | 0.3420 | 0.3413 | 0.3407 | 0.3406 | 0.3408 | 0.3408 | 0.3410 | 0.3419 |
| Prompts | | Idx10 | Idx11 | Idx12 | Idx13 | Idx14 | Idx15 | Idx16 | Idx17 | Idx18 | Idx19 |
| GOES2Radar | RMSE | 0.4711 | 0.4762 | 0.4731 | 0.4706 | 0.4743 | 0.4752 | 0.4747 | 0.4764 | 0.4735 | 0.4725 |
| | CSI | 0.3260 | 0.3252 | 0.3277 | 0.3266 | 0.3264 | 0.3297 | 0.3248 | 0.3247 | 0.3276 | 0.3265 |
| Radar Extrapolation | RMSE | 0.4927 | 0.4931 | 0.4934 | 0.493 | 0.4938 | 0.4929 | 0.4932 | 0.4934 | 0.4937 | 0.4934 |
| | CSI | 0.2478 | 0.2474 | 0.2483 | 0.2483 | 0.2493 | 0.2488 | 0.2474 | 0.2477 | 0.2479 | 0.2474 |
| GOES-IR2GOES-IR | RMSE | 0.4052 | 0.3017 | 0.2917 | 0.3136 | 0.3027 | 0.2828 | 0.2886 | 0.3189 | 0.3147 | 0.3102 |
| | CSI | 0.6451 | 0.7057 | 0.7034 | 0.6930 | 0.7064 | 0.7044 | 0.7076 | 0.6899 | 0.6982 | 0.7040 |
| Radar Spatial SR | RMSE | 0.1332 | 0.1333 | 0.1332 | 0.1332 | 0.1332 | 0.1332 | 0.1332 | 0.1333 | 0.1332 | 0.1332 |
| | CSI | 0.7222 | 0.7221 | 0.7215 | 0.7216 | 0.7217 | 0.7219 | 0.7218 | 0.7215 | 0.7224 | 0.7213 |
| Radar Temporal SR | RMSE | 0.3166 | 0.3168 | 0.3167 | 0.3168 | 0.3166 | 0.3167 | 0.3166 | 0.3169 | 0.317 | 0.3166 |
| | CSI | 0.3359 | 0.3374 | 0.3370 | 0.3371 | 0.3381 | 0.3367 | 0.3375 | 0.3374 | 0.3371 | 0.3376 |
| Deblur | RMSE | 0.2252 | 0.2233 | 0.2272 | 0.2257 | 0.2259 | 0.2257 | 0.2264 | 0.2267 | 0.2235 | 0.2263 |
| | CSI | 0.3405 | 0.3405 | 0.3413 | 0.3417 | 0.3416 | 0.3418 | 0.3416 | 0.3417 | 0.3414 | 0.3415 |

D MORE VISUAL RESULTS

To comprehensively assess the performance of WeatherGFM, we present a range of qualitative visual results across various tasks, including weather forecasting, weather super-resolution, and weather image translation. Additionally, we conduct a comparative evaluation against the unified ViT-large model, as well as single-task ViT and UNet models. The visual outputs and comparisons are thoughtfully illustrated in Figure 10.

WeatherGFM’s proficiency in generating visually appealing outputs is readily evident in the presented results. Notably, the visual quality surpasses that of the baseline models. However, the significance of WeatherGFM’s capability extends beyond visual quality. Its distinctive strength lies in its ability to effectively handle a wide array of image enhancement tasks and image detection. This marks a noteworthy distinction from traditional models, which often struggle to concurrently address such a diverse spectrum of tasks.

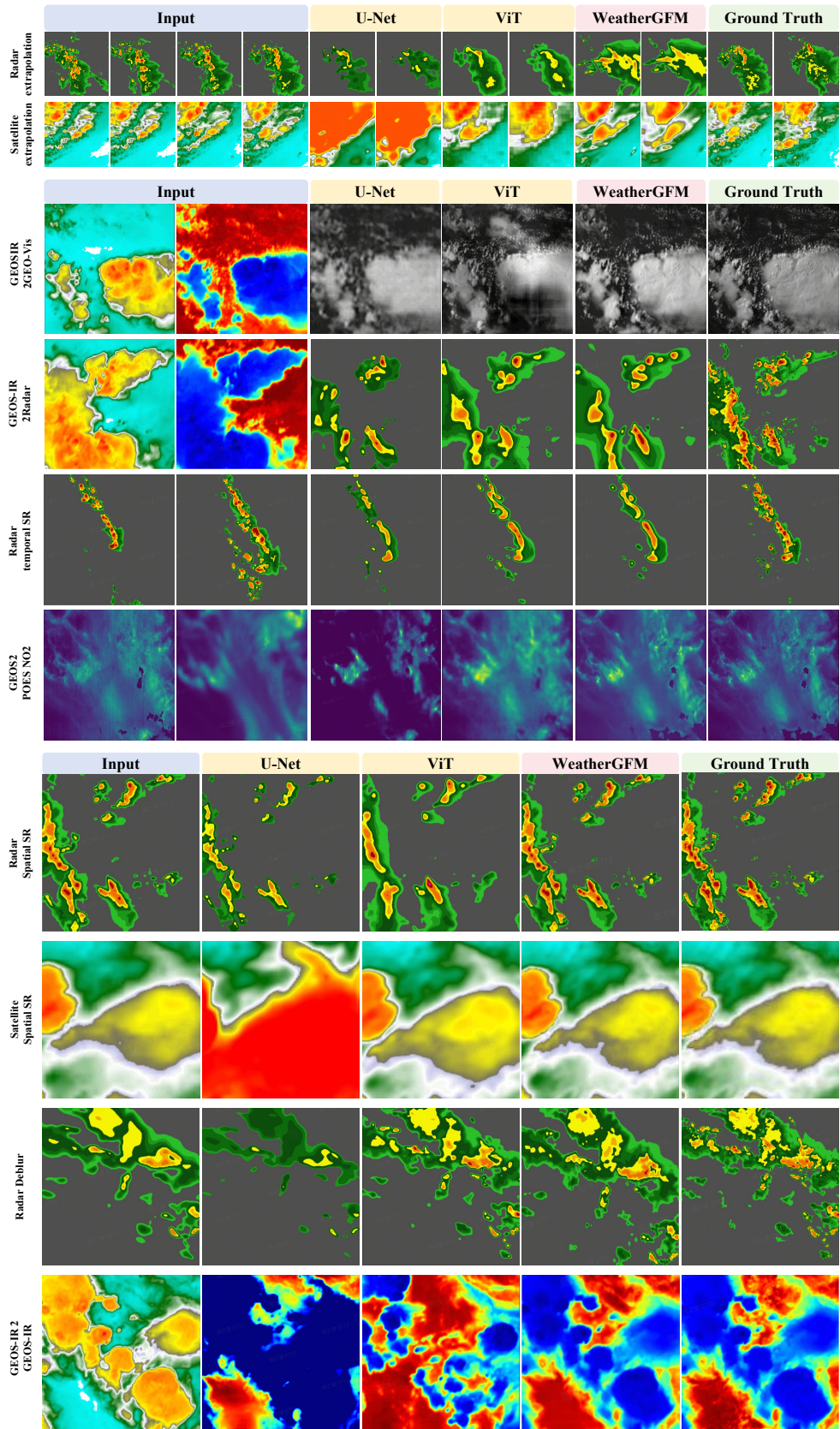


Figure 10: Visual results of the weather understanding tasks by our WeatherGFM.

Table 6: More quantitative results on weather understanding tasks. We also report the results of the POD and FAR metrics.

| Task name | Downscaling | | | | | | Forecasting | |
|------------|----------------------|--------|-------------------|--------|------------------|--------|---------------------|--------|
| | Satellite Spatial SR | | Radar Temporal SR | | Radar Spatial SR | | Radar Extrapolation | |
| Metrics | POD | FAR | POD | FAR | POD | FAR | POD | FAR |
| UNet | 1.0000 | 0.7466 | 0.4380 | 0.1738 | 0.6568 | 0.1702 | 0.3207 | 0.1751 |
| ViT | 0.9941 | 0.0560 | 0.4520 | 0.0139 | 0.7219 | 0.0047 | 0.2749 | 0.0228 |
| WeatherGFM | 0.9973 | 0.0540 | 0.4362 | 0.0111 | 0.7320 | 0.0039 | 0.3028 | 0.0162 |

| Task name | Inversion | | | | | | Forecasting | |
|------------|------------|--------|----------------------|--------|---------------|--------|-------------------------|--------|
| | GOES2Radar | | GOES-IR2GOES-Visible | | GOES2POES-NO2 | | Satellite Extrapolation | |
| Metrics | POD | FAR | POD | FAR | POD | FAR | POD | FAR |
| UNet | 0.4691 | 0.1821 | 0.4260 | 0.1358 | 0.5993 | 0.2548 | 1.0000 | 0.7841 |
| ViT | 0.3537 | 0.0229 | 0.4626 | 0.0829 | 0.5421 | 0.1686 | 0.9599 | 0.3514 |
| WeatherGFM | 0.3524 | 0.0147 | 0.3630 | 0.1388 | 0.5023 | 0.0024 | 0.9578 | 0.2379 |

E ADDITIONAL QUANTITATIVE RESULTS

In this section, we present more quantitative results on various weather understanding tasks. The results include the Probability of Detection (POD) and False Alarm Rate (FAR) metrics for different models across multiple tasks. Table 6 provides a detailed comparison of these metrics for the UNet, ViT, and WeatherGFM models. AVG.POD and AVG.FAR represent the mean scores across different thresholds for various tasks. For radar output tasks, the thresholds are [16, 74, 133, 160, 181, 219]; for GEOS-visible output tasks, the thresholds are [2000, 3200, 4400, 5600, 6800]; and for GEOS-IR069 output tasks, the thresholds are [-4000, -5000, -6000, -7000].